Stability behaviour of a cylindrical rocket engine combustion chamber operated with liquid hydrogen and liquid oxygen

S. Gröning⋆,⋆⋆, D. Suslov⋆, M. Oschwald⋆, and T. Sattelmayer⋆⋆
⋆German Aerospace Centre (DLR), Lampoldshausen
Im Langen Grund 1, 74239 Hardthausen, Germany
⋆⋆Lehrstuhl für Thermodynamik, Technische Universität München
Boltzmannstraße 15, 85748, Garching

Abstract

High frequency combustion instabilities in liquid propellant rocket engines are investigated using a subscale rocket engine with the propellant combination hydrogen/oxygen at representative conditions. It has been demonstrated in previous test runs with this combustion chamber that it shows self-excited high frequency combustion instabilities at specific operating conditions with gaseous hydrogen at a temperature of 115 K. In order to investigate the effect of the hydrogen temperature, this analysis has been expanded to test runs with liquid hydrogen. It is shown that the hydrogen temperature has a significant influence on the acoustic behaviour of the combustion chamber and therefore on the observed instabilities.

1. Introduction

High frequency combustion instabilities in liquid propellant rocket engines are a problem which has been known of since the beginning of the construction of these engines [20]. Because of the complexity of the processes involved, the phenomenon is still not completely understood. For this reason, models intended to predict the stability behaviour of liquid propellant rocket engines have had limited success. The pressure oscillations produced by the combustion have a broad frequency spectrum and can therefore be considered as noise. The combustion chamber reacts to this broadband acoustic excitation with the oscillation of its eigenmodes. These eigenmode oscillations in turn have an effect on the combustion. If the combustion processes are sensitive to one of the eigenfrequencies of the combustion chamber, the combustion starts to oscillate as well, which causes a periodic modulation of the heat release of the flame. Rayleigh discovered that the energy transfer between the heat release and pressure fluctuations depends on the phase shift between these two oscillations [14]. When the phase shift becomes zero, a maximum energy transfer between heat release and the acoustic pressure oscillations occurs, causing a rapid increase of the amplitudes of the oscillations. High amplitude pressure oscillations increase the heat transfer from the hot combustion gases into the combustion chamber wall. In the worst case, this increased heat transfer cannot be compensated by the cooling system, causing a destruction of the combustion chamber wall and therefore of the whole engine. This phenomenon is called combustion instabilities [6, 23].

The key factor for understanding these instabilities lies in the understanding of the coupling mechanisms between the acoustics and the combustion as these processes determine the rate of energy transfer [13]. Basic coupling mechanisms have been discovered so far, but the current understanding does not allow an accurate prediction of the instability behaviour of a combustion chamber. The strategies used to avoid combustion instabilities still have an empirical background. To ensure the stability of a rocket engine expensive full scale tests are required. If combustion instabilities are discovered during these tests, they are addressed by installing damping devices or changing the injector geometry until a stable design is found.

Experimental investigations of combustion instabilities are usually performed with model combustion chambers specially designed for this purpose. Examples of such model combustion chambers are those operated at the German Aerospace Centre (DLR), at the Technical University of Munich (TUM), at ONERA in France, at Purdue University [22] and Pennsylvania State University [11] in the USA. At DLR Lampoldshausen the “Common Research Chamber” (CRC) [8] as well as the combustion chamber model “H” (BKH) [5] are used for the investigation of combustion instabilities. At ONERA the “Multiple Injector Combustor” (MIC) as well as the “Very High Amplitude Modulator” (VHAM) [15] are operated. At the Technical University of Munich, acoustic investigations with cold flow test benches are performed [7].

The aim of the investigations performed with these model combustion chambers is to identify the coupling mechanisms between acoustics and the combustion [5]. All model combustion chambers mentioned in the previous paragraph use an external excitation system to produce a known acoustic field with high amplitudes in order to analyse the reaction of the flame to these oscillations. The advantage of these systems is that the acoustic pressure field is known and can be controlled. On the other hand the acoustic excitations are forced by an external system and not by the combustion itself. The approach shown in this paper is a different one. The experiments presented here were performed with a subscale combustion chamber named BKD (combustion chamber model "D") with the injector head L-42 [19]. In previous work it has been shown, that this combustion chamber shows self-excited high frequency combustion instabilities for specific operating conditions [4]. For this reason the combustion chamber has been equipped with appropriate measurement elements and tested over a large range of operating conditions in order to investigate the dependence of these self-excited combustion instabilities on operating conditions. Previously, one test run with gaseous hydrogen with a temperature of around 115 K has already been analysed [4]. In this paper the analysis is extended to more test runs, including test runs with liquid hydrogen, in order to investigate the effect of hydrogen temperature on the stability behaviour of the combustion chamber. When the terms gaseous and liquid hydrogen are used here, this means from which tank of the test bench the hydrogen was taken. In the gaseous hydrogen tank, the hydrogen is stored at ambient temperature with high pressure. In the liquid hydrogen tank the hydrogen is stored cryogenically. In the injection manifold of the combustor, hydrogen is, strictly speaking, a supercritical fluid. The abbreviations GH and LH are used here simply to distinguish the high and low temperature ranges of injected hydrogen.

2. Experimental Setup

The main advantages of the investigation with the experimental combustor BKD are the representative conditions which can be achieved inside the combustion chamber and the self-excited combustion instabilities which appear at sepcific operating conditions. Representative in this case means that the BKD combustion chamber with the injector head L-42 is a multi injector engine with 42 shear coaxial injectors and is operated with the cryogenic fuel combination liquid oxygen/hydrogen (LOX/H_2). The maximum combustion chamber pressure is 80 bar, which means that the liquid oxygen is in a super critical condition. The combustion chamber has a cylindrical shape with a diameter of 80 mm, which allows rotating tangential modes to occur [24], [17]. The combustion chamber BKD is operated at the P8 test bench the research and technology test bench for cryogenic high pressure combustion at DLR Lampoldshausen [19].

The main focus of the test runs presented in this paper is the measurement of the acoustic pressure oscillations inside the combustion chamber. For this reason a special HF measurement ring was installed between the injector head and the combustion chamber (see Fig. 1, left). The right illustration in Fig. 1 shows a more detailed representation of this HF measurement ring. The main measurement elements are the 8 dynamic pressure sensors which are installed flush mounted around the circumference of the ring with an equiangular distance of 45°. The measurement plane of the ring is located 5.5 mm behind the faceplate of the injector head.

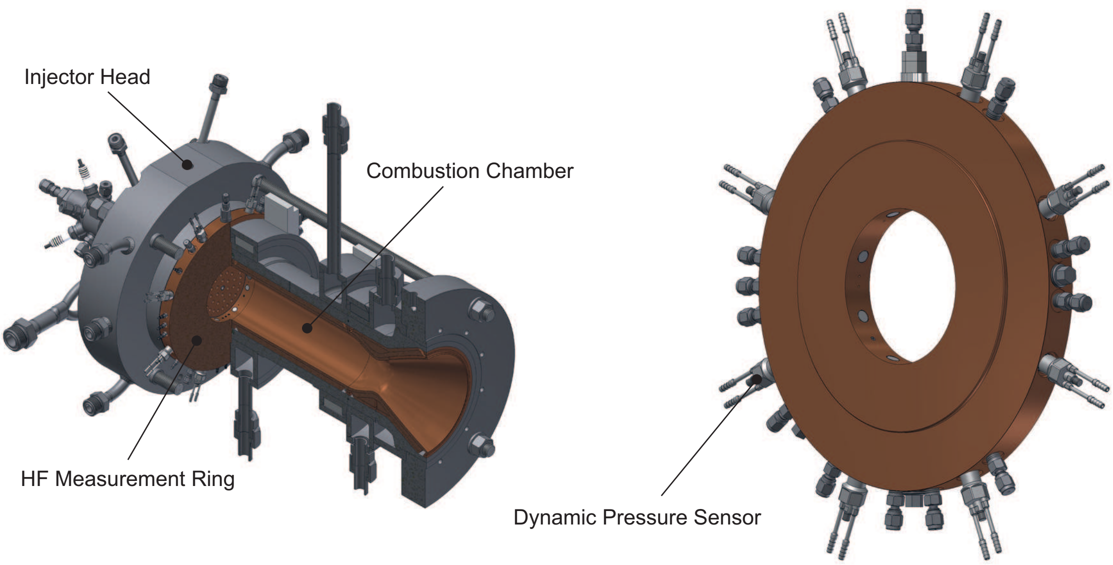

Figure 1: Combustion Chamber BKD with HF measurement ring installed bewteen the injector head and the combustion chamber (left). HF measurement ring with 8 flush mounted dynamic pressure sensors (right)

In this paper, the analysis of a total number of seven test runs including test runs with gaseous (GH) and liquid hydrogen (LH), which were conducted in two different test campaigns, is presented. Each test run consists of several different load points. Each load point is defined by a combustion chamber pressure p_{cc} and a value of the mixture ratio ROF = $\dot{m}_{O_2}/\dot{m}_{H_2}$ [4] with $\dot{m}_{O_2}$ being the oxygen massflow and $\dot{m}_{H_2}$ the hydrogen massflow. All together, the analysis in this paper includes a total number of 92 load points. 50 of these were obtained from test runs with gaseous hydrogen and 42 from test runs with liquid hydrogen. The acquired data set has been analysed to examine the dependence of the acoustic oscillations on combustion chamber pressure p_{cc}, mixture ratio ROF and hydrogen temperature T_{H2}.

3. Data Analysis

The data obtained during the two test campaigns has been used for an intensive analysis with the aim to characterise the acoustic behaviour and its dependence on operating conditions. The analysis presented here is the direct continuation of the analysis shown in [4], extended to more test runs, including different hydrogen temperatures. Therefore the results of the analysis presented here not only show the dependence of the acoustic oscillations on different load points but also the dependence on hydrogen temperature. It will be shown in the following sections, that the hydrogen temperature has a significant effect on the acoustic behaviour of the combustion chamber. It was demonstrated, that the combustion chamber BKD with the injector head L-42 shows for specific operating conditions high amplitude pressure oscillations of the first tangential mode [4]. Fig. 2 shows a comparison of a test run with gaseous hydrogen (GH, left) and liquid hydrogen (LH, right). In the top axis, the value of a gliding RMS is plotted. This RMS value represents the average amplitude of the dynamic pressure sensor signal for a time window of 0.2 s. The dynamic pressure sensor signal from which the RMS values were obtained is plotted in the second axis. The third axis shows the signals of the combustion chamber pressure p_{cc}, the mixture ratio ROF, and the hydrogen temperature T_{H2}, and therefore the sequence of the test run. On the right side of Fig. 2 the same information is plotted for a test run with liquid hydrogen. In general, the dynamic pressure sensor signal shows lower amplitudes compared to the test run with gaseous hydrogen. An important observation is, that the observed high amplitude osciallations for the load point p_{cc}=80 bar, ROF 6 in the GH case, which is an instability of the first tangential eigenmode [4], are not present for the same load point in the LH case. This shows that the hydrogen temperature has a significant influence on the acoustic behaviour of the combustion chamber. The strong oscillations between 70 and 75 s in the GH case are not a 1T instability but a low frequency coupling with the feed system. In the following sections these aspects will be analysed in more detail. In general, all test runs showed consistent results and comparable trends with good reproducibility.

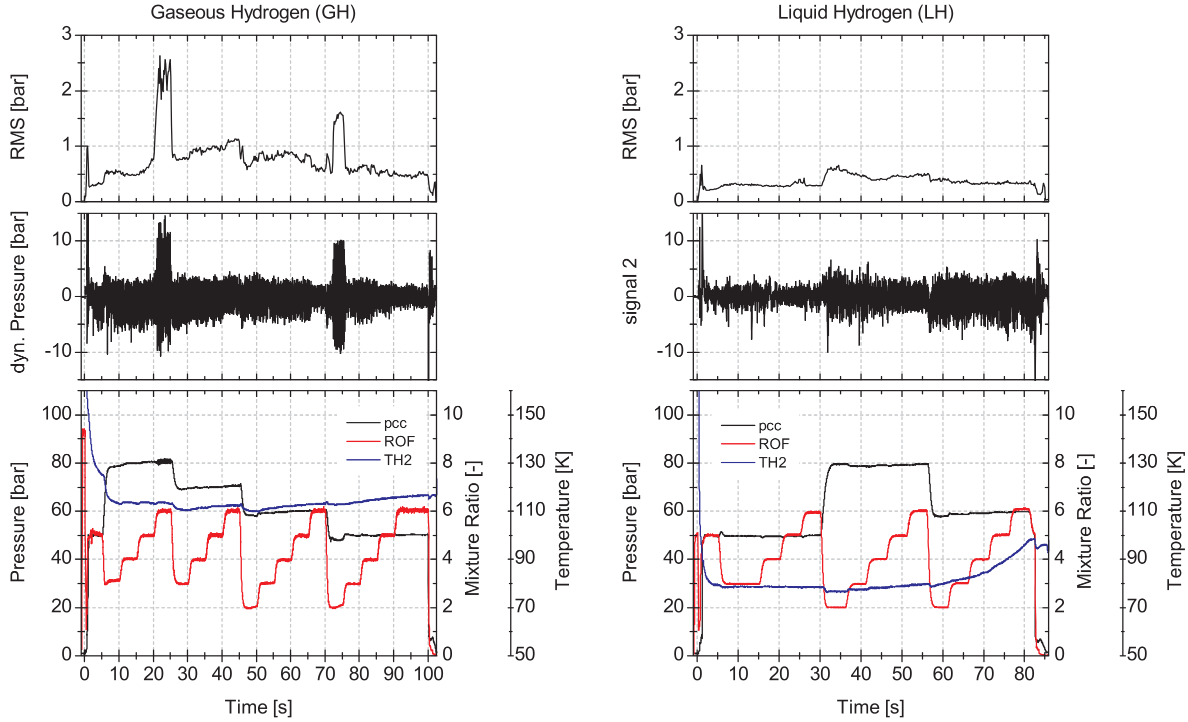

Figure 2: Gliding RMS of the acoustic oscillations as a function of the different operating conditions

3.1 Mode Identification

Every volume defined by solid walls and filled with a fluid has specific eigenfrequencies which are defined by the geometry of the walls and the properties of the medium. The differential equation which describes the pressure fields of the acoustic eigenmodes is the 3-dimensional wave equation [24].

$$\frac{\partial^2 p}{\partial t^2} = a^2 \,\Delta p \tag{1}$$

where a is the speed of sound, t the time, and p the acoustic pressure. For the geometry of a closed circular cylinder, the 3-dimensional wave equation can be solved analytically as shown in [24]. The solution of Eq. (1) for a cylindrical geometry is the equation for the acoustic pressure field $p(r, \theta, t)$ with r and θ being the cylinder coordinates as well as the equation for the eigenfrequencies

$$f_{m,n,q} = \frac{a}{2}\sqrt{\left(\frac{\alpha_{mn}}{R}\right)^2 + \left(\frac{q}{L}\right)^2} \tag{2}$$

where R is the radius and L the length of the cylinder. The symbols m, n, and q are the wave numbers for which any positive integer or zero can be chosen. The longitudinal modes are described by the wave number q, the tangential modes by n and the radial modes by m. When two of the wave numbers are zero, the eigenmode is called a pure mode. If for example $m = n = 0$ and $q = 1$ the frequency of the first longitudinal (1L) mode is obtained by Eq. (2). If $q = 2$, the mode is called the second longitudinal (2L) which is a higher harmonic of the first longitudinal mode. In this paper the following terminology will be used: xL for the x^{th} longitudinal mode, xT for the x^{th} tangential mode and xR for the x^{th} radial mode. Besides the pure modes exist also the so called combination modes. These modes are created by a combination of two or three wave numbers. A mode with $m = 0$, $n = 1$ and $q = 1$ for example would be called a 1T1L mode. The values for α_{mn} are the solutions of

$$\frac{\partial J_n(\pi\alpha_{mn})}{\partial r} = 0 \tag{3}$$

and therefore are the roots of the Bessel function of the first kind of the n^{th} order, divided by π. The values for α_{mn} are tabulated in [24]. Eq. (2) can therefore be used to calculate the eigenfrequencies of a cylindrical volume, providing that the geometry and the speed of sound is known. It has to be considered, that the combustion chamber of a rocket engine has a cylindrical shape but is not a pure cylinder which is assumed for Eq. (2). The main deviations from the pure cylindrical geometry are the injector head and the nozzle, which are attached at both ends of the cylindrical combustion chamber volume. Another, non-geometric but even more important deviation from Eq. (2) is the speed of sound a. In Eq. (2) a constant speed of sound over the whole volume of the cylinder is assumed. The speed of sound inside a combustion chamber varies in space as the gas properties inside the chamber are nonuniform. It has been shown, that despite these deviations it is possible to identify most of the dominant eigenfrequencies measured in the BKD combustion chamber as pure eigenmodes of a cylinder [4]. Fig. 3 shows a typical power spectral density of a dynamic pressure sensor signal measured in the combustion chamber BKD. The shown frequencies were calculated using Eq. (2) with $R = 40$ mm, $L = 225$ mm and $a = 1420$ m/s [4]. The most dominant peaks which can be seen in Fig. 3 therefore correspond to the eigenfrequencies of a cylinder and because of this, result from the cylindrical volume of the combustion chamber. Other peaks could not be identified yet. A more detailed discussion of some of these unknown eigenfrequencies is given in section 3.3.

Fig. 4 shows two spectrograms, one resulting from a test run with gaseous hydrogen (GH, left) and one resulting from a test run with liquid hydrogen (LH, right). Under the spectrograms, the dynamic pressure sensor signals which have been used to calculate the spectrograms are shown. Under the dynamic pressure sensor signals the signals of the combustion chamber pressure p_{cc}, the mixture ratio ROF and the hydrogen temperature T_{H2} can be seen. During the test run with gaseous hydrogen, the hydrogen temperature had an average value of around 115 K. The test run with liquid hydrogen shows an average temperature of around 80 K in the beginning and towards the end of the test run an increase to around 100 K. This increase results from the pressurisation of the liquid hydrogen tank. At the end of the test, the tank runs out of liquid hydrogen which then causes an increase of the temperature as more and more gaseous hydrogen is mixed in. The temperature difference between the gaseous and liquid hydrogen case is just 35 K but as will be shown in this paper, this already has a significant effect on the acoustics of the combustion chamber.

In the left spectrogram of Fig. 4, resulting from a test run with gaseous hydrogen (GH), the 1T mode can be seen as a broad line around 10 kHz. The three broad lines above the 1T mode are the 2T, 3T and 4T mode. Below the 1T line, the 1L mode around 3 kHz and the 2L mode around 6 kHz can be seen. By observing the spectrogram of the GH test run, one aspect immediately stands out: The eigenfrequencies of the chamber change with the operating conditions. The test sequence consists of four pressure steps and in each pressure step the ROF is varied. If the spectrogram is analysed

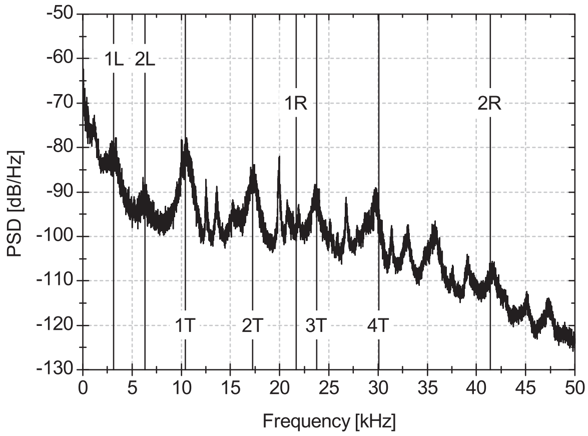

Figure 3: Mode identification by comparing the PSD of a dynamic pressure sensor signal with the analytically calculated eigenfrequencies of a cylinder [4]

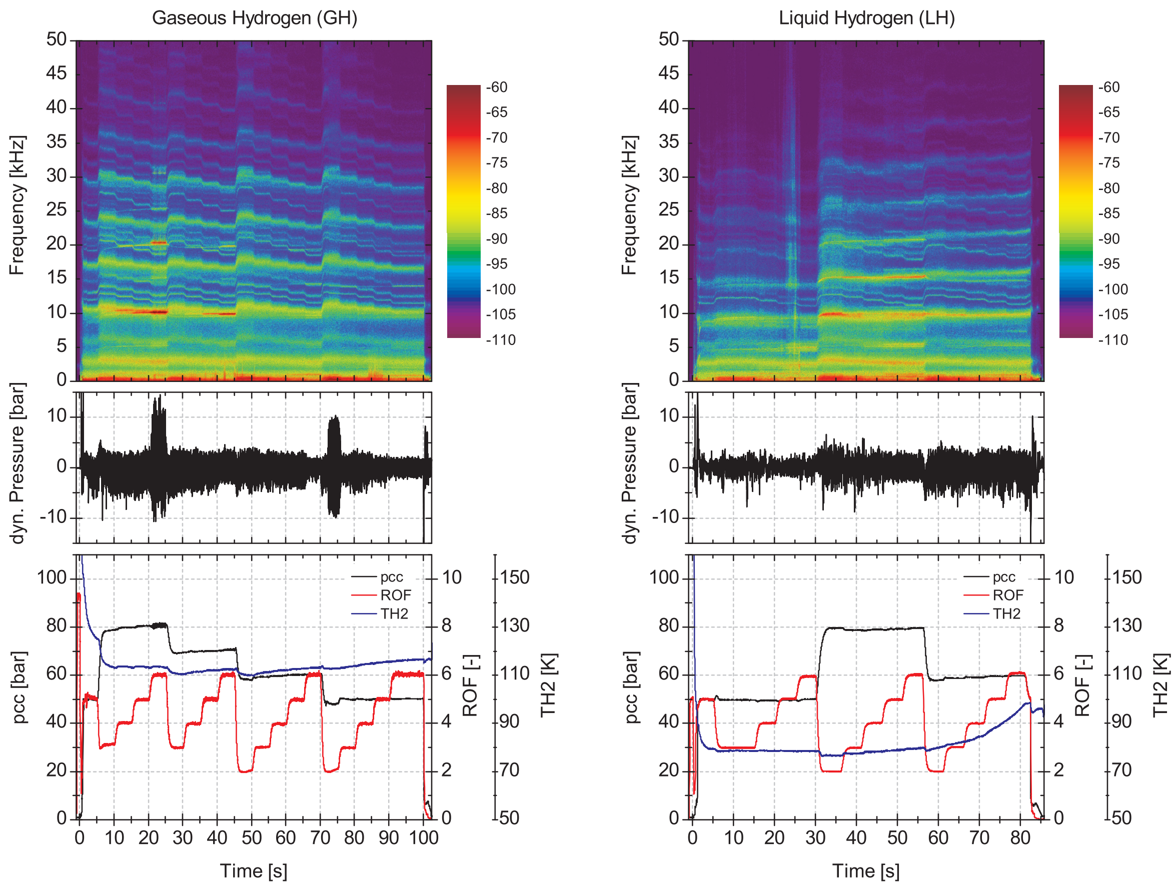

Figure 4: Spectrorams of a test run with gaseous hydrogen (GH, left) and liquid hydrogen (LH, right)

carefully one can see that the chamber frequencies are dependent on pressure and ROF with a greater sensitivity to ROF. From this observation it can be concluded that the change in frequency is caused by a change in the speed of sound inside the combustion chamber which is dependent on both, pressure and mixture ratio. The dependence of the speed of sound on operating conditions is analysed in more detail in section 3.2.

When the gaseous hydrogen (GH) spectrogram (Fig. 4, left) is compared with the liquid hydrogen (LH) spectrogram, some similarities as well as some differences can be observed. First of all the same eigenmodes can be discovered, although in the LH case they are less clear compared to the GH case. This mainly results from the lower overall amplitudes of the dynamic pressure sensor signals in the LH case which becomes clear when the two dynamic pressure sensor signals in Fig. 4 are compared. Again, the 1T mode occurs approximately at 10 kHz, however at the beginning of the test run the 1T frequency is lower compared to the GH case. As in the GH case, three broad lines above the 1T line can be seen, belonging to the 2T, 3T and 4T mode. Below the 1T line, the 1L and the 2L mode can be found again. The 2L line which is around 6 kHz should not be mistaken with another very thin line at around 5 kHz. As can be seen in both spectrograms, for some operating conditions very sharp lines at 5, 10, 15, 20 kHz etc. are visible. These lines are assumed to result from the LOX system as the slight change in their frequencies corresponds to the change of the speed of sound of liquid oxygen. The LOX system frequencies might play a role in the instabilities observed in the BKD combustor with the L-42 injector head, because for unstable load points the 10 kHz line of the LOX system coincides with the line of the 1T mode of the combustion chamber. But as this would be out of the scope of this paper, these lines will not be considered furthermore at this point.

Another interesting feature, which can be observed from the two spectrograms are three very sharp lines between the 1T and the 2T mode. As the origin of these lines could not be clarified yet, they will be named x1, x2 and x3 mode in this paper (see also Fig. 5). In the spectrogram of the LH test run, the highest of these three lines (x3) is often not visible, as it is very close to the line of the 2T mode in this case. In the GH case, where the hydrogen temperature is more constant than in the LH case, it can be observed that the ratios of the tangential modes to these x-modes are constant. When the tangential modes frequencies change, the x-modes change their frequencies in the same way. In the LH case, a different behaviour can be observed towards the end of the test run, when the hydrogen temperature starts to increase at around 55 s. It can be seen that the tangential mode frequencies follow the change of the hydrogen temperature: When the hydrogen temperature starts to increase, so do the frequencies of the tangential modes. The x-modes on the other hand seem not to be affected by the change of the hydrogen temperature. This aspect will be analysed in more detail in section 3.3.

Fig. 5 shows two PSDs, one calculated for the dynamic pressure sensor signals of a gaseous hydrogen (GH) test run and one for a liquid hydrogen (LH) test run. The PSDs were calculated using the Welch method [21] with a Hanning window [1, 18]. The data is from the same test runs as the spectrograms in Fig. 4. For each PSD a time window of one second has been extracted out of all eight dynamic pressure sensor signals of the HF measurement ring. For each signal, the averaged PSD over one second has been calculated and averaged over the eight sensors to obtain one PSD for the defined time window. For the GH case the time window was set from 89 to 90 s and for the LH case from 4 to 5 s. This corresponds to the 50 bar, ROF 5 load point for both, GH and LH cases. These load points were selected for showing an example PSD as there is only little interference with other modes. In the GH case (Fig. 5, left), the cylinder frequencies (1L, 2L, 1T, 2T, 3T, 4T) are clearly visible as well as the three x-modes (x1, x2, x3). The sharp peak between the x2 and the x3 mode belongs to the frequencies which are assumed to result from the LOX system (see Fig. 4). In the LH case only the 1L, 2L, 1T, 2T and 4T as well as the x1 and x2 modes are clearly visible. The 3T mode is too weak to be clearly distinguished. By comparing the two PSDs in Fig. 5 it can be seen that the resonant frequencies in the LH case are lower than in the GH case.

3.2 Dependence of the Speed of Sound on Operating Conditions

From the spectrograms of section 3.1 it has been observed that the eigenfrequencies are dependent on the operating conditions. This means that the speed of sound inside the combustion chamber is dependent on the operating conditions. The following relationships have already been identified by the analysis of the spectrograms:

- The speed of sound decreases with an increase of the mixture ratio (ROF)
- The speed of sound depends on the combustion chamber pressure (p_{cc}) but the dependence is small and not clear
- The speed of sound decreases with a decrease of the hydrogen temperature (T_{H2})
- The pressure dependence is much weaker than the mixture ratio and hydrogen temperature sensitivity

These dependencies are analysed in more detail in this section. As has been already mentioned in section 3.1 the acoustic behaviour of the combustion chamber can be explained using the equations for a pure circular cylinder (Eq. 2).

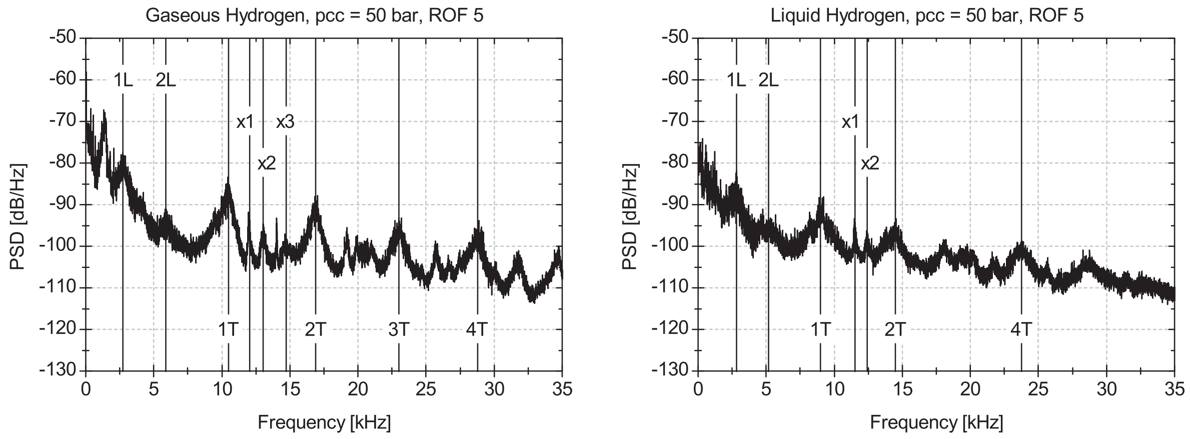

Figure 5: Power spectral density (PSD) calculations of a test run with gaseous hydrogen (left) and liquid hydrogen (right)

It is therefore possible to create a substitute cylinder with a specified radius R, length L, and speed of sound a, which has the same eigenfreqeuncies as the combustion chamber. The procedure of creating this substitute cylinder consists of the following steps: The radius of the cylinder is known as it is identical to the radius of the combustion chamber. The length of the cylinder is unknown, as the combustion chamber is not a pure cylinder but has a nozzle attached to one end which increases the length of the combustion chamber but cannot be simplified as an extension of the length of the cylinder by the length of the nozzle. Also the injector head affects the acoustic length of the cylindrical part. Actually the length L of the substitute cylinder is a virtual measure which describes the ratio of the longitudinal to the tangential modes for a given speed of sound. The speed of sound is unknown as it has been explained in section 3.1. Also the speed of sound of the substitute cylinder is a virtual measure and should not be mistaken for the actual speed of sound in the combustion chamber which is nonuniform. The speed of sound of the substitute cylinder is such that it produces the same eigenfrequencies of the substitute cylinder compared to the measured ones in the combustion chamber. It can be interpretetd as an average speed of sound approximating the nonuniform speed of sound distribution inside the combustion chamber.
The eigenfrequencies of the combustion chamber can be determined for every load point by calculating an average PSD for the load point and measuring the positions of the peaks. Hence there exists for every load point a set of frequencies: $f_{1L,\mathrm{exp}}$, $f_{2L,\mathrm{exp}}$, $f_{1T,\mathrm{exp}}$, $f_{2T,\mathrm{exp}}$ etc. If an eigenfrequency cannot be determined from the PSD because it is unclear which peak is the correct one, this eigenmode is ignored. The procedure of creating the substitute cylinder can then be transformed into a system of equations using Eq. (2):

$$\frac{a}{2}\frac{1}{L} = f_{1L,\mathrm{exp}} \tag{4}$$

$$\frac{a}{2}\frac{2}{L} = f_{2L,\mathrm{exp}} \tag{5}$$

$$\vdots$$

$$\frac{a}{2}\frac{\alpha_{01}}{R} = f_{1T,\mathrm{exp}} \tag{6}$$

$$\frac{a}{2}\frac{\alpha_{02}}{R} = f_{2T,\mathrm{exp}} \tag{7}$$

$$\vdots$$

This equation system can then be transformed into a least squares optimisation problem

$$\min_{\bar{x}} \|\bar{f}_{sc} - \bar{f}_{\mathrm{exp}}\|_2^2 \tag{8}$$

$\bar{f}_{sc}$ is a vector containing the eigenfrequencies of the substitute cylinder calculated using Eq. (2), $\bar{f}_{\mathrm{exp}}$ is a vector containing the eigenfrequencies measured from the PSD and $\bar{x}$ being the vector with the optimisation variables.

$$\bar{x} = \begin{pmatrix} L \\ a \end{pmatrix} \tag{9}$$

This optimisation problem is then solved using a reflective trust region algorithm [2]. As a result of this optimisation procedure, a length L and a speed of sound a are obtained which minimise the difference between the eigenfrequencies of the substitute cylinder and the measured eigenfrequencies. It would be also possible to include the radius R in the vector $\bar{x}$ of optimisation variables, but in this case the optimisation problem would have an infinite number of solutions. As a result of this procedure, for every load point of every test run a set of a and L has been calculated.
Fig. 6 shows the calculated speed of sound of the substitute cylinder plotted against the mixture ratio ROF. Each symbol corresponds to a combustion chamber pressure level combined with a hydrogen temperature. For the gaseous hydrogen cases (GH) Fig. 6 represents very well what has already been derived from the spectrograms in Fig. 4: The speed of sound decreases with increasing mixture ratio. There is also a very weak dependence on the combustion chamber pressure: Decreasing the chamber pressure causes a slight decrease in the speed of sound, but the effect is negligible compared to the effect of increasing the mixture ratio. The data points of the liquid hydrogen case show a greater spreading than the data points of the gaseous hydrogen test runs. This can be easily explained as follows: The PSD data of the LH test runs in general is more difficult to read because the peaks of the eigenmodes are less clear which results mainly from the lower amplitudes of the oscillations. Therefore the experimentally obtained frequencies have a larger error which has an influence on the speed of sound calculated with Eq. (8). Furthermore the hydrogen temperature is less constant in a liquid hydrogen test run. Especially at the end of the test run when the hydrogen temperature increases as has been shown in Fig. 4. As the hydrogen temperature also influences the speed of sound only data points with a nearly constant hydrogen temperature are included in this plot. In general, the same observations can be made for the liquid hydrogen test run as have been made for the gaseous hydrogen test runs. Increasing the ROF decreases the speed of sound. Also the weak pressure dependence can be observed in the data points of the LH test runs. By comparing the data points of the GH and LH test runs it can be observed that the hydrogen temperature has an even stronger effect on the speed of sound than the mixture ratio.

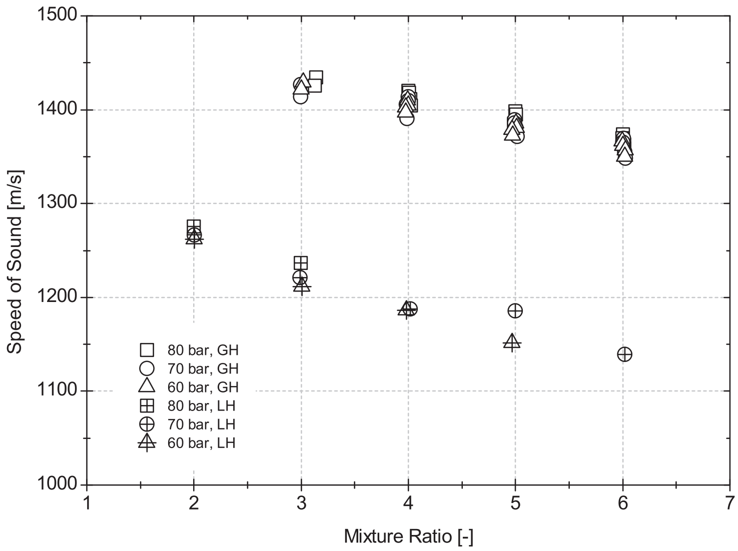

Figure 6: Speed of sound a of the substitute cylinder plotted against the mixture ratio for test runs with gaseous (GH) and liquid hydrogen (LH)

The observations made concerning the dependence of the speed of sound on the mixture ratio ROF, the combustion chamber pressure p_{cc} and the hydrogen temperature T_{H2} can be explained theoretically. For an ideal gas, the speed of sound is given by [16]

$$a = \sqrt{\gamma \frac{p}{\rho}} = \sqrt{\gamma R_s T} \quad (10)$$

where p is the pressure, ρ the density, γ the heat capacity ratio, R_s the specific gas constant and T the temperature. If the specific gas constant is replaced by the universal gas constant the following equation is obtained [10]:

$$a = \sqrt{\gamma \frac{R}{M} T} \quad (11)$$

where R is the universal gas constant and M the molar mass of the gas. If the mixture ratio is increased the temperature T is increased (see Fig. 7) and therefore the speed of sound should also be increased. It must be considered that the molar mass changes as well with the ROF. The average molar mass M of a mixture of ideal gases is given by the sum of the molar masses of each species multiplied with the mole fractions x of the species [10]. The gas mixture after the combustion consists of hydrogen and water. The molar mass of this gas mixture therefore is given by

$$M = x_{H_2} M_{H_2} + x_{H_2O} M_{H_2O} \tag{12}$$

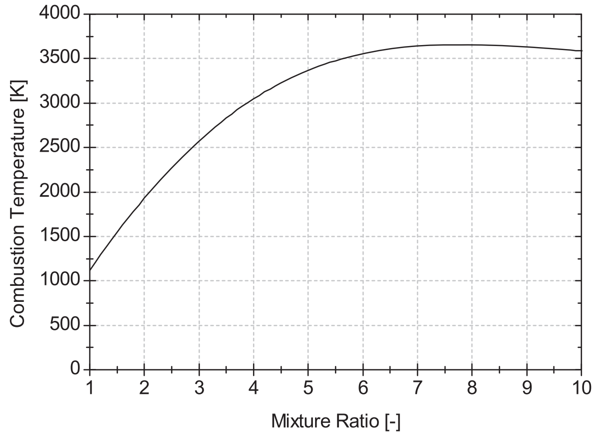

Figure 7: Dependence of the combustion temperature of hydrogen and oxygen on the mixture ratio ROF [3]

The molar mass of water (M_{H_2O} = 18.015 g/mol) is much higher than the molar mass of hydrogen (M_{H_2} = 2.0159 g/mol) [9]. When the ROF is increased, the mole fraction of hydrogen x_{H_2} decreases whilst the mole fraction of water x_{H_2O} increases. According to Eq. (12) this leads to an increase of the molar mass of the mixture which again leads to a decrease of the speed of sound according to Eq. (11). In the end, the effect of the molar mass is stronger than the change of the temperature due to the ROF change. If for example the ROF is changed from 2 to 6, the temperature increases by a factor of 1.8 (see Fig. 7). But the molar mass increases by a factor of 2.3, so in the end the speed of sound decreases. Therefore an increase of the ROF causes an increase of the molar mass of the combustion gases which results in a decrease of the speed of sound and of the eigenfrequencies.
The observed effects can also be proven by the calculation of the speed of sound of the combustion chamber gases using the NASA CEA code [3]. Fig. 8 shows the speed of sound and its dependence on the mixture ratio ROF and the combustion chamber pressure p_{cc}. As can be seen in Fig. 8, the speed of sound increases with an increase of the combustion chamber pressure. But the effect is quite small compared to the effect of the mixture ratio ROF. This is in agreement with the experimental observations. That an increase of the pressure causes an increase of the speed of sound can also be directly concluded from Eq. (10)

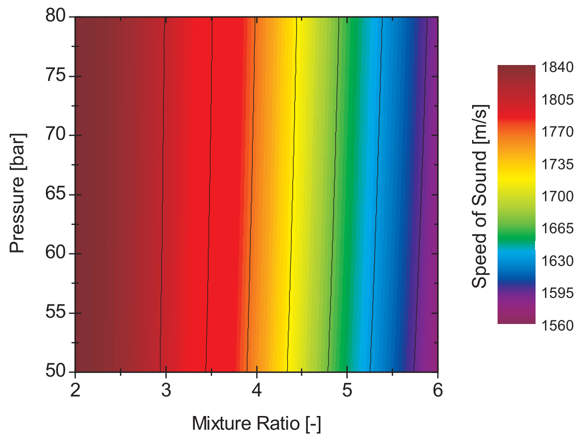

Figure 8: Dependence of the speed of sound of the combustion gases of hydrogen and oxygen on the mixture ratio ROF and the combustion chamber pressure p_{cc} [3]

The effect of hydrogen temperature is easy to understand. With a lower hydrogen temperature the temperature especially in the area close to the faceplate decreases significantly. Also the temperature of the combustion gases decreases, as more energy is required to heat up the hydrogen. All in all, the decrease of the hydrogen temperature causes a decrease of the temperature of the gases in the combustion chamber which leads to a reduction of the speed of sound according to Eq. (10).

3.3 Frequency Ratios

It has been described in section 3.1, that it is difficult to compare theoretically calculated eigenfrequencies for a pure cylinder (see Eq. (2)) with experimentally obtained eigenfreqeuncies as the speed of sound inside the combustion chamber is nonuniform and therefore difficult to predict. Another method of comparing theoretical and experimental eigenfrequencies which does not have this disadvantage is to compare the ratios between the eigenfrequencies. As can be derived from Eq. (2), the ratios of the eigenfrequencies of a pure cylinder are all independent to the speed of sound and depend only on physical constants or the geometry of the cylinder. The ratio of the frequency of the 2T mode to the frequency of the 1T mode for example is

$$\frac{f_{2\mathrm{T}}}{f_{1\mathrm{T}}} = \frac{\alpha_{02}}{\alpha_{01}} \tag{13}$$

The ratio of the frequency of the 1T mode to the 1L mode is

$$\frac{f_{1\mathrm{T}}}{f_{1\mathrm{L}}} = \alpha_{01}\frac{L}{R} \tag{14}$$

Furthermore this means, that the ratios of the experimentally obtained eigenfrequencies should also be independent to the speed of sound and therefore be constant for all load points. These frequency ratios can be calculated for the known eigenmodes as well as for the x-modes (x1, x2 and x3) between the 1T and 2T mode. Fig. 9 shows the ratios $f_{2\mathrm{T}}/f_{1\mathrm{T}}$, $f_{3\mathrm{T}}/f_{2\mathrm{T}}$, $f_{4\mathrm{T}}/f_{3\mathrm{T}}$, $f_{\mathrm{x}2}/f_{\mathrm{x}1}$ and $f_{\mathrm{x}3}/f_{\mathrm{x}1}$, which were derived from the experimentally measured eigenfrequencies, plotted against the hydrogen temperature. As predicted by Eq. (2), these values are independent to the load points.

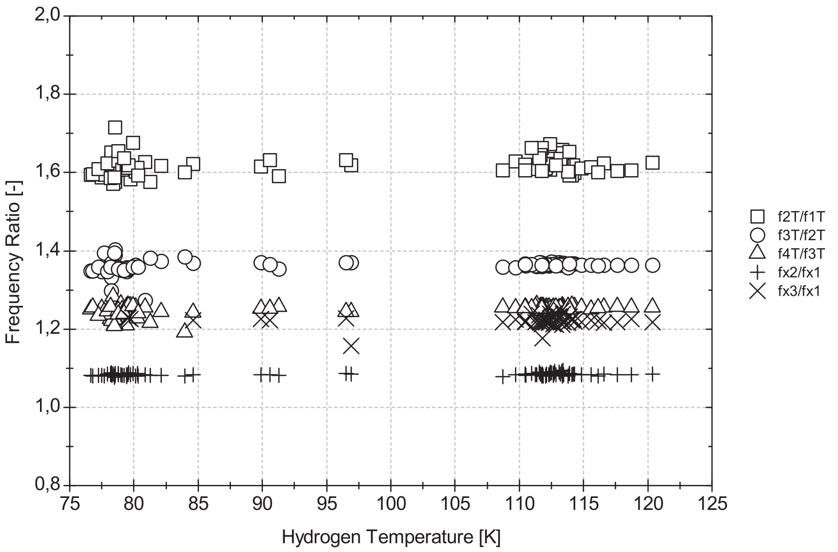

Figure 9: Experimentally obtained frequency ratios

Tab. 1 gives a summary of the averaged values of these frequency ratios. As the origin of the x-modes is not identified yet, these frequency ratios cannot be calculated theoretically. The ratios of the tangential modes on the other hand only depend on the α_{mn} values and can therefore be calculated. Tab. 1 shows also a comparison of the theoretically and experimentally obtained ratios of the tangential modes as well as the absolute and relative difference. The theoretical and experimental values are not perfectly identical but show reasonable agreement. This demonstrates that the simple model of a pure cylinder is already a good representation of the acoustics inside the combustion chamber.
In Fig. 9 the tangential modes were only compared to tangential modes and the x-modes only compared to x-modes. The spectrogram of the liquid hydrogen test run in Fig. 4 (right) has already shown that the tangential modes and the x-modes show a difference in the dependence on hydrogen temperature. As the tangential modes follow the increase of the hydrogen temperature, the x-modes seem not to be affected by it. This means, that the ratios between the tangential modes and the x-modes are not constant but depend on hydrogen temperature. This dependence is shown in Fig. 10,

Table 1: Mean values of the experimentally obtained frequency ratios compared to the frequency ratios of a pure cylinder

	Experimental	**Theoretical**	**Difference**	**rel. Difference**
f_{2T}/f_{1T}	1.618	1.659	0.041	2.47 %
f_{3T}/f_{2T}	1.362	1.376	0.013	0.97 %
f_{4T}/f_{3T}	1.249	1.266	0.017	1.38 %
f_{x2}/f_{x1}	1.084			
f_{x3}/f_{x1}	1.224			

where the ratios of the 1st, 2nd, 3rd and 4th tangential mode to the x1 mode are plotted against the hydrogen temperature. In general, the spreading of the data points is higher compared to the ratios shown in Fig. 9. But the dependence of these ratios is clearly visible: With lower hydrogen temperatures these ratios decrease. For temperatures above 110 K they seem to remain constant. This dependence on hydrogen temperature shows that the origin of the x-modes must be different to that of the tangential modes. A possible source could be the hydrogen manifold as the hydrogen speed of sound is nearly independent of the temperature for the typical manifold pressures of the L-42 injector head. Therefore the hydrogen temperature changes the speed of sound of the combustion chamber, as has been shown in section 3.2, while the speed of sound in the hydrogen manifold remains nearly constant.

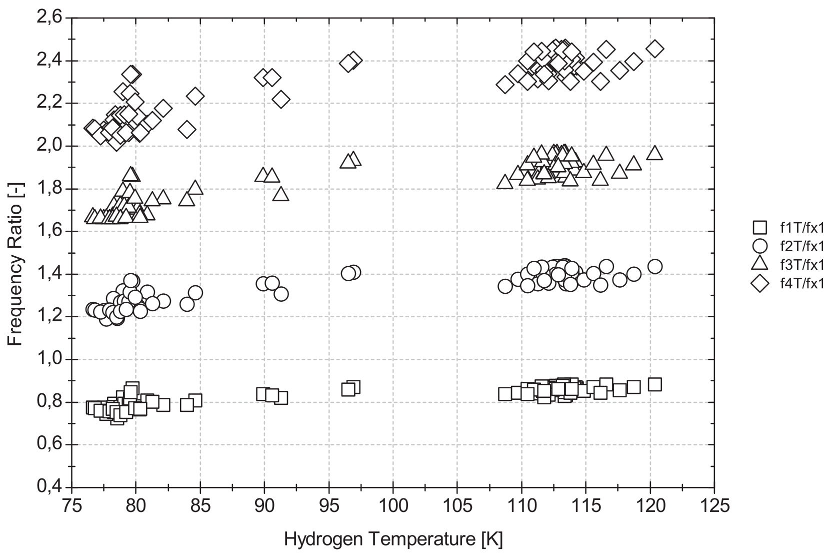

Figure 10: Experimentally obtained frequency ratios of tangential modes to x-modes

3.4 Oscillation amplitudes and their dependence on hydrogen temperature

A detailed analysis of the oscillation amplitudes as a function of the operating conditions was performed for one test run with gaseous hydrogen [4]. This analysis has now been expanded to all seven test runs including the GH and LH runs. The focus here will be on the dependence of the amplitudes on hydrogen temperature. The basic idea of this analysis is, that specific frequency bands are extracted out of the raw dynamic pressure sensor signals from which the RMS values are calculated in order to get a value for the average amplitude of the oscillations in this frequency band for every load point. Fig. 11 shows the RMS values of the unfiltered dynamic pressure sensor signals for all 92 load points. As can be seen, there is a slight trend, that with lower hydrogen temperatures the RMS values decrease. For the GH test runs 4 points with significantly higher RMS values of around 2.5 bar can be seen. For all GH test runs this is the load point p_{cc} = 80 bar, ROF 6 which showed reproducible high amplitude 1T oscillations in all four GH test runs (see also [4]). But as there are many other load points with the same hydrogen temperature this cannot be attributed to the hydrogen temperature alone. Also for the LH test runs one load point with a significantly higher RMS value of 5 bar, which is twice as high as the 1T oscillations of the GH runs was observed. This RMS value was obtained for the load point p_{cc} = 80 bar, ROF 2 at a hydrogen temperature of approximately 80 K.
If a band pass filter centered on the frequency of the 1T mode is applied to the raw dynamic pressure sensor signals, only the oscillations of the 1T mode are extracted. The RMS values calculated for these band pass filtered signals

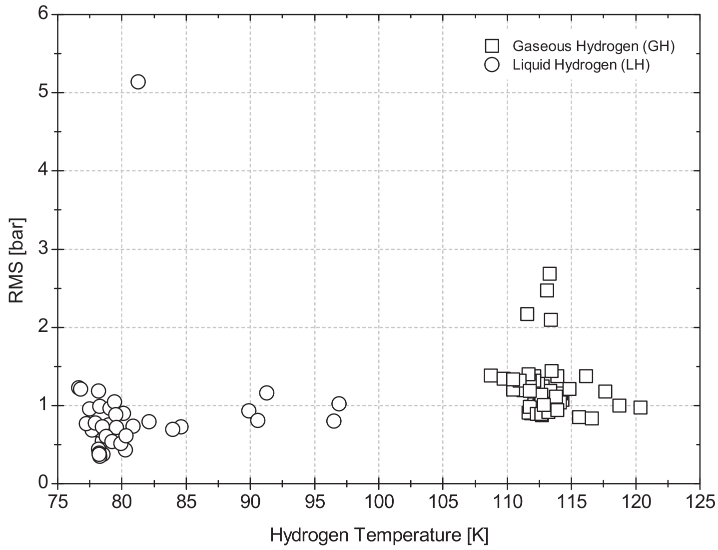

Figure 11: RMS values of the raw dynamic pressure sensor signals

show the average oscillation amplitude of the 1T mode for every load point. In Fig. 12, the left diagram shows the RMS values of the 1T mode for all 92 load points, plotted against the hydrogen temperature. The filter used here is a Butterworth band pass filter of second order [12]. 87 % of the load points show 1T RMS values of under 0.5 bar. But also in Fig. 12, some load points with significant higher RMS values of the 1T mode can be discovered. Again, the RMS values around 2 bar are the four $p_{cc} = 80$ bar, ROF 6 load points of the GH test runs. The load point with the highest 1T RMS value of around 4.7 bar is again the $p_{cc} = 80$ bar, ROF 2 load point of the LH test run. This shows, that similar to the other case, the observed oscillations result from a significant instability of the 1T mode, as the RMS value of the 1T mode in this case is nearly 100 % of the RMS value of the raw signal. Furthermore it can be concluded from Fig. 12 that the observed instability of the 1T mode is not caused by the hydrogen temperature, as several load points exist with the same hydrogen temperatures of the unstable load points with very low RMS values of the 1T mode.

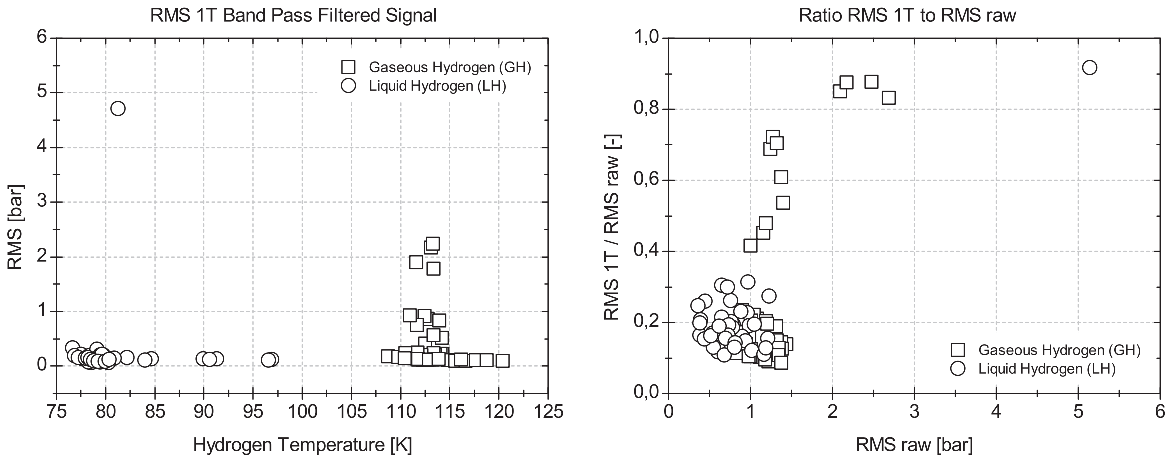

Figure 12: RMS values of 1T mode (left). Ratio of the 1T RMS values to the RMS values of the raw signal (right)

The right diagram in Fig. 12 shows the ratio of the RMS values of the 1T mode to the RMS values of the raw signal, plotted against the RMS values of the raw signal. As can be seen in Fig. 12, for most load points, this factor is around 0.15. But as soon as the RMS values of the raw signal increase, this ratio increases and becomes nearly 1 for the strongest oscillations. This shows that whenever a strong oscillation is observed in the BKD combustion chamber it is primarily caused by the 1T mode. This conclusion has previously been stated before [4], when one test run with 9 load points was analysed. From the new results this observation has been confirmed by further analysis of the other test runs.

3.5 Pressure Field Reconstruction

A pressure field reconstruction method, which is able to reconstruct the amplitude and orientation of the first tangential mode in the plane of the sensors (see Fig. 13), based on the dynamic pressure sensor signals measured on the combustion chamber wall, has been presented by Sliphorst et. al. [17]. It was also shown, that the analytical solution of the wave equation (Eq. (1)) allows standing 1T modes, rotating 1T modes with a constant angular velocity, and an infinite number of rotating 1T modes with a non-constant angular velocity to exist.

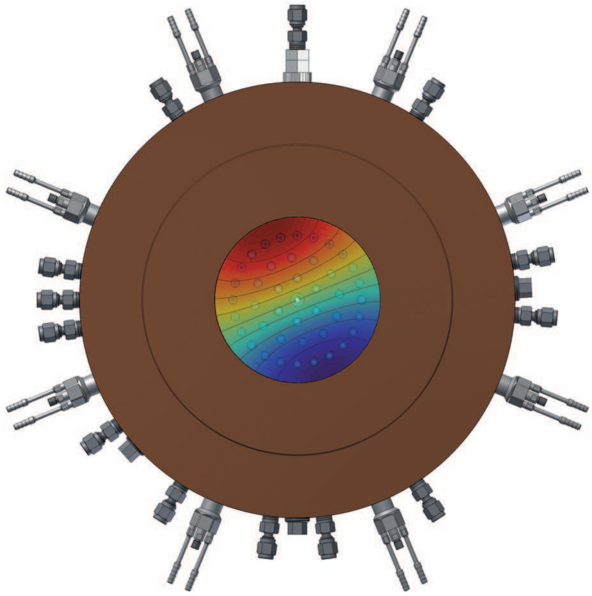

Figure 13: 1T mode in the plane of the measurement ring, defined by the positions of the dynamic pressure sensors

This pressure field reconstruction method has been applied to the dynamic pressure sensor signals of a test run with the BKD combustion chamber with gaseous hydrogen [4]. A rotation parameter Φ has been introduced, which is a measure for the average rotation characteristics of the 1T mode for a specific load point. This rotation parameter is a function of the time t and therefore represents the current rotation type of the 1T mode. If $\Phi = 0$ the pressure field of the 1T mode is a standing wave. For $\Phi > 0$ the pressure field of the 1T mode shows a clock wise rotation whilst for $\Phi < 0$ the rotation is counter-clockwise. If $\Phi = 1$ or $\Phi = -1$ the rotation has a constant angular velocity. As the value of Φ tends towards zero, the more irregular the rotation becomes. In the limiting case of $\Phi = 0$ the rotation turns into a standing wave with fixed positions of the nodes and anti-nodes of the 1T pressure field.
If the absolute values of Φ are taken and averaged over the time frame of one load point the average rotation character of the 1T mode can be calculated. By taking the absolute value of Φ, the information about the rotation direction is lost, but the information about the rotation character can still be obtained. If the averaged value of $|\Phi|$ is close to 1, this means the average rotation character is close to a rotating wave with constant angular velocity. If the averaged value of $|\Phi|$ is closer to 0 on the other hand, the rotation character of this load point is closer to a standing 1T mode.
It was shown, that the averaged rotation character depends on the amplitude of the 1T mode [4]. For higher amplitudes of the 1T mode, lower values of $|\Phi|$ were observed. This means for stronger 1T oscillations the rotation character of the 1T mode tends more towards a standing wave. Therefore the unstable load points show a stronger tendency towards a standing wave, while all other load points show very similar values of $|\Phi|$ and therefore similar rotation characters. This observation has already been made for one test run with gaseous hydrogen [4]. This analysis has been expanded in the current work to more test runs, including test runs with liquid hydrogen. Fig.14 shows the averaged values of $|\Phi|$, plotted against the amplitude of the 1T mode. The same tendency as described before [4] has been observed for the load points of the new test runs.

4. Summary and Conclusions

The analysis presented in this paper was focused on the influence of hydrogen temperature on the acoustic behaviour of the combustion chamber. It was shown that the mixture ratio ROF, the combustion chamber pressure p_{cc} and the hydrogen temperature T_{H2} affect the speed of sound inside the combustion chamber and therefore the eigenfrequencies.

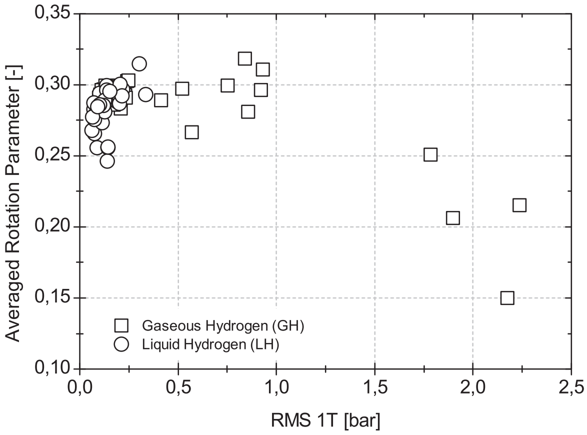

Figure 14: Averaged rotation parameter $|\Phi|$ of the 1T mode and its dependence on the RMS values of the 1T mode

The effect of the combustion chamber pressure is low compared to the effect of the mixture ratio and the hydrogen temperature. Furthermore it was demonstrated that the frequency ratios of the tangential modes of the combustion chamber are independent of operating conditions. The experimentally observed values of these frequency ratios agree well with the theoretically predicted values. Next to the cylinder modes of the combustion chamber three eigenmodes with unknown origin, and therefore named x-modes, were analysed. It was shown that the ratio of these x-modes is also constant and independent of operating conditions. On the other hand the ratio of the tangential modes of the combustion chamber to these x-modes shows a dependence on hydrogen temperature. This indicates that the x-modes must result from another volume than the combustion chamber.
The average amplitude of the 1T mode for every analysed load point has been calculated using a band pass filter in combination with a RMS calculation. It was shown that as soon as strong oscillations appear in the combustion chamber the oscillation is primarily dominated by an oscillation of the 1T mode. However this was determined to not be an effect of hydrogen temperature. Unstable load points with high RMS values of the 1T mode where observed for both test runs with gaseous and with liquid hydrogen. Furthermore, other load points with the same hydrogen temperature showed only low RMS values of the 1T mode. The hydrogen temperature alone does not cause the observed instabilities, but it changes the load points where the instabilities appear. A load point which shows 1T oscillations with high amplitudes in the GH test runs shows no significant 1T amplitudes in the LH test runs. However, the highest observed 1T amplitudes were discovered in one load point of the LH test runs. The fact that the instabilities occur at different operating conditions for GH and LH test runs can be explained by the strong influence of the hydrogen temperature on the combustion chamber eigenfrequencies.
The dependence of the eigenfrequencies of the combustion chamber can also be seen in the spectrograms shown in Fig. 4. For some operating conditions very sharp lines at the frequencies of 5, 10, 15, 20 kHz etc. have been discovered. These lines show only a little dependence on the operating conditions but seem to play a role as soon as the combustion chamber hits an unstable load point. As the slight changes of the frequencies of these lines match the change of the speed of sound of the liquid oxygen it seems that these lines must be a result of the LOX system. In this case the observed instabilities of the 1T mode would be a coupling of the 1T mode with the LOX system. Further analysis is currently being conducted to investigate this assumption.
The combustion chamber can be divided into three different systems, with three different values for the speed of sound: The combustion chamber with the combustion gases, the hydrogen manifold, filled with hydrogen and the LOX manifold, filled with liquid oxygen. By changing the operating conditions the values for the speed of sound in these three different systems are changed, but in different ways. It seems that in the combustion chamber not only eigenmodes of the cylindrical part of the chamber can be seen, but also eigenmodes resulting from the propellant manifolds. As the lines of the spectrograms in Fig. 4 are dependent on the operating conditions in different ways this information can be used to distinguish from which system the observed frequencies are resulting.

Acknowledgements

The Authors are grateful to the crew of the P8 test bench as well as Philipp Groß and Mike Ziemßen for their efforts in performing the test runs on which the results presented here are based. Research undertaken for this paper has been assisted with financial support from the DFG (Deutsche Forschungsgemeinschaft) in the framework of the SFB-TR 40.

References

[1] Bendat, J. and A. G. Piersol. 1993. Engineering Applications of Correlation and Spectral Analysis. John Wiley & Sons. New York.

[2] Conn, A. R., N. I. M. Gould, and P. L. Toint. 2000. Trust-Region Methods. Society for Industrial and Applied Mathematics and Mathematical Programming Society. Philadelphia.

[3] Gordon, S. and B. J. McBride. 1994. Computer program for calculation of complex chemical equilibrium compositions and applications. Part 1: Analysis. NASA-RP-1311. National Aeronautics and Space Administration.

[4] Gröning, S., M. Oschwald, and T. Sattelmayer. 2012. Selbst erregte tangentiale Moden in einer Raketenbrennkammer unter repräsentativen Bedingungen. In: *61. Deutscher Luft- und Raumfahrtkongress*.

[5] Hardi, J., M. Oschwald, and B. Dally. 2011. Flame Response to acoustic excitation in a rectangular rocket combustor with LOx/H_2 propellants. *CEAS Space Journal* 2: 41–49.

[6] Harrje, D. and F. Reardon (Eds.). 1972. Liquid Propellant Rocket Combustion Instability. SP-194. National Aeronautics and Space Administration.

[7] Kathan, R., D. Morgenweck, R. Kaess and T. Sattelmayer. 2011. Validation of the Computation of Rocket Nozzle Admittances with Linearized Euler Equations. In: *4th European Conference for Aerospace Sciences*.

[8] Knapp, B., Z. Farago, and M. Oschwald. 2007. Interaction of LOX/GH_2 Spray-Combustion with Acoustics. In: *45th AIAA Aerospace Sciences Meeting and Exhibit*.

[9] Linstrom, P. J. and W. G. Mallard (Eds.). 2013. NIST Chemistry WebBook, NIST Standard Reference Database Number 69. National Institute of Standards and Technology. Gaithersburg.

[10] Lucas, K. 2004. Thermodynamik. Springer-Verlag. Berlin.

[11] Marshall, W., S. Pal, R. Woodward, R. J. Santoro, R. Smith, G. Xia, V. Sankaran, and C. L. Merkle. 2006. Experimental and Computational Investigation of Combustor Acoustics and Instabilities, Part II: Transverse Modes. In: *44th AIAA Aerospace Sciences Meeting & Exhibit*.

[12] Oppenheim, A. V. and R. W. Schafer. 1975. Digital Signal Processing. Prentice Hall.

[13] Putnam, A. A. 1971. Combustion-driven Oscillations in Industry. American Elsevier Publishing Company. New York.

[14] Rayleigh, J. W. S. 1878. The explanation of certain acoustic phenomena. *Nature* 18:319–321.

[15] Rey, C., S. Ducruix, P. Scouflaire, L. Vingert, and S. Candel. 2004. High Frequency Combustion Instabilities Associated with Collective Interactions in Liquid Propulsion. In: *40th AIAA/ASME/SAE/ASEE Joint Propulsion Conference & Exhibit*.

[16] Rossing, T. D. (Ed.). 2007. Springer Handbook of Acoustics. Springer Science+Business Media. New York.

[17] Sliphorst, M., S. Gröning, and M. Oschwald. 2011. Theoretical and Experimental Identification of Acoustic Spinning Mode in a Cylindrical Combustor. *Journal of Propulsion and Power* 27:182–189.

[18] Stearns, S. D. 1975. Digital Signal Analyis. Hayden Book Company. Rochelle Park.

[19] Suslov, D., A. Woschnak, J. Sender, and M. Oschwald. 2003. Test Specimen Design and Measurement Technique for Investigation of Heat Transfer Processes in Cooling Channels of Rocket Engines Under Real Thermal Conditions. In: *39th AIAA/ASME/SAE/ASEE Joint Propulsion Conference & Exhibit*.

[20] Sutton, G. P. and O. Biblarz. 2001. Rocket Propulsion Elements. John Wiley & Sons. New York.

[21] Welch, P. D. 1967. The use of fast Fourier transform for the estimation of power spectra: A method based on time averaging over short, modified periodograms. *IEEE Transactions on Audio and Electroacoustics* 15:70–73.

[22] Xia, G., M. Harvazinski, W. Anderson, and C. L. Merkle. 2011. Investigation of Modeling and Physical Parameters on Instability Prediction in a Model Rocket Combustor. In: *47th AIAA/ASME/SAE/ASEE Joint Propulsion Conference & Exhibit*.

[23] Yang, V. and W. Anderson (Eds.). 1995. Liquid Rocket Engine Combustion Instability. *Progress in Astronautics and Aeronautics* Vol. 169, American Institute of Aeronautics and Astronautics.

[24] Zucrow, M. J. and J. D. Hoffman. 1985. Gas Dynamics, Volume II. Krieger Publishing Company. Malabar.